PDMS stamps were inked with $C_{16}SH$ by rubbing the surfaces of stamps with a cotton swab pre-soaked with a solution of 20 mM [27] $C_{16}SH$ in ethanol followed by drying in a stream of nitrogen. The patterned SAMs were formed by pressing the inked stamps in contact with the gold substrates for about 1 min. The substrate was then washed with ethanol and DI water and blown dry in N_2 stream.

Underpotential Deposition: The procedure for underpotentially depositing silver and copper has been described previously [8]. For the upd of copper onto gold, the working electrode was cycled at a rate of 10 mV s^{-1} from 0 to 450 mV and emersed from the electrochemical cell under a controlled potential on the third anodic scan at 135 mV (vs. Cu wire) for $\phi_{Cu} = 0.6$. For the upd of silver, the working electrode was cycled at 10 mV s^{-1} from 0 to 650 mV and emersed under a controlled potential on the third cathodic scan at 60 mV (vs. Ag wire) for $\phi_{Ag} = 0.9$. After emersion, the substrates were rinsed with absolute ethanol and blown dry in a N_2 stream. The coverages of the upd adlayers were determined by XPS as described previously [24].

Desorption of SAMs: The SAM-patterned electrodes were cycled at 50 mV s^{-1} from 0.05 V to –1.4 V (vs. Ag/AgCl) in 0.5 M KOH in ethanol to reductively desorb the SAMs from the substrates [17]. During the final scan, the potential was held at –1.4 V and the substrate was removed from the electrochemical cell under controlled potential. The sample was rinsed with absolute ethanol and blown dry in a N_2 stream.

Formation of PM Patterns: Dilute solutions of diazomethane in ether were carefully prepared according to a literature procedure [28]. Warning: diazomethane is highly explosive and highly toxic and should be handled with extreme care. The concentration of diazomethane in ether was determined by titration with benzoic acid. Substrates were placed in an ethereal solution containing a desired concentration of DM for a predetermined period of time at 0 °C. The amount of time the samples were exposed to air after emersion from the electrochemical cell and prior to DM exposure was ~ 1–2 min.

Characterization: AFM images of PM films were obtained with a Nanoscope III scanning probe microscope (SPM) equipped with a J piezoelectric scanner (Digital Instruments, Santa Barbara, CA). An area of 120 × 120 μm^2 was scanned in tapping mode to attain the height images under an ambient laboratory environment. The images were plane fitted and filtered to remove noise using the instrument software.

Received: January 14, 2003
Final version: February 14, 2003

[1] S. D. Ittle, L. K. Johnson, *Chem. Rev.* **2000**, *100*, 1169.
[2] *Polymer Data Handbook* (Ed: J. E. Mark), Oxford University Press, New York **1999**.
[3] *Polymer Handbook* (Eds: J. Brandrup, E. H. Immergut, E. A. Grulke), 4th ed., Wiley, New York **1999**.
[4] J. S. Kong, D. J. Lee, H. D. Kim, *J. Appl. Polym. Sci.* **2001**, *82,* 1677.
[5] K. Seshadri, S. V. Atre, Y.-T. Tao, M.-T. Lee, D. L. Allara, *J. Am. Chem. Soc.* **1997**, *119*, 4698.
[6] Y.-T. Tao, K. Pandian, W.-C. Lee, *Langmuir* **1998**, *14,* 6158.
[7] A. Kumar, H. A. Biebuyck, G. M. Whitesides, *Langmuir* **1994**, *10*, 1498.
[8] W. Guo, G. K. Jennings, *Langmuir* **2002**, *18*, 3123.
[9] S. Manne, P. K. Hansma, J. Massie, V. B. Elings, A. A. Gewirth, *Science* **1991**, *251*, 183.
[10] C.-H. Chen, S. M. Vesecky, A. A. Gewirth, *J. Am. Chem. Soc.* **1992**, *114*, 451.
[11] T. Hachiya, H. Honbo, K. Itaya, *J. Electroanal. Chem.* **1991**, *315*, 275.
[12] D. M. Kolb, in *Advances in Electrochemistry and Electrochemical Engineering* (Eds: H. Gerischer, C. W. Tobias), Wiley, New York **1978**, Vol. 11, pp. 125–275.
[13] Y. Zhang, Y. Sung, P. A. Rikvold, A. Wieckowski, *J. Chem. Phys.* **1996**, *104*, 5699.
[14] Y. Nakai, M. S. Zei, D. M. Kolb, G. Lehmpfuhl, *Ber. Bunsenges. Phys. Chem.* **1984**, *88*, 340.
[15] D. Oyamatsu, S. Kuwabata, H. Yoneyama, *J. Electroanal. Chem.* **1999**, *473*, 59.
[16] D. E. Weisshaar, B. D. Lamp, M. D. Porter, *J. Am. Chem. Soc.* **1992**, *114*, 5860.
[17] C. A. Widrig, C. Chung, M. D. Porter, *J. Electroanal. Chem.* **1991**, *310*, 335.
[18] R. J. Jackman, D. C. Duffy, E. Ostuni, N. D. Willmore, G. M. Whitesides, *Anal. Chem.* **1998**, *70*, 2280.
[19] A. P. Russo, D. Apoga, N. Dowell, W. Shain, A. M. P. Turner, H. G. Craighead, H. C. Hoch, J. N. Turner, *Biomed. Microdevices* **2002**, *4*, 277.
[20] E. Shinohara, S. Kondo, K. Akahori, K. Tashiro, S. Shoji, *IEICE Trans. Electron.* **2001**, *E84-C*, 1897.
[21] S. A. Campbell, *The Science and Engineering of Microelectronic Fabrication*, Oxford University Press, New York **1996**.
[22] J. Tien, Y. Xia, G. M. Whitesides, in *Thin Films* (Ed: A. Ulman), Academic Press, Boston, MA **1998**, Vol. 24, pp. 227–254.
[23] After exposure to 10 mM DM in ether at 0 °C for 15 h, the following ellipsometric thicknesses were obtained for PM films: 947 nm on Cu(upd)/Au ($\phi_{Cu} = 0.6$); 770 nm on $C_{16}S$/Cu(upd)/Au ($\phi_{Cu} = 0.6$); 54 nm on Au; 205 nm on $C_{16}S$/Au; 0 nm on Ag(upd)/Au ($\phi_{Ag} = 0.9$). These results indicate that a SAM actually enhances PM film growth on gold upon long-term exposures to DM in ether.
[24] G. K. Jennings, P. E. Laibinis, *J. Am. Chem. Soc.* **1997**, *118*, 5208.
[25] F. P. Zamborini, J. K. Campbell, R. M. Crooks, *Langmuir* **1998**, *14*, 640.
[26] We conducted an experiment to deposit Ag(upd) on a Cu(upd)/Au surface that has a complete monolayer derived from $C_{16}SH$. The cyclic voltammogram showed no silver deposition or stripping peaks in the potential range of –0.05 to 0.75 V (vs. Ag wire). This result agrees with those from Oyamatsu [15] that long chain alkanethiols prevent metal ions from diffusing to the substrate surface. Next, we electrochemically desorbed the $C_{16}S$-SAM in a 0.5 M KOH/ethanol solution at –1.4 V (vs. Ag/AgCl) and placed the substrate into a 0.1 M H_2SO_4(aq) solution to electrochemically desorb Cu(upd). That the observed intensity of the desorbing peak of copper was approximately the same (within 5 %) as that of the deposition peak of copper during the original upd process indicates that a $C_{16}S$ monolayer protects the underlying Cu(upd) adatoms from desorption during the Ag(upd) process.
[27] D. J. Graham, D. D. Price, B. D. Ratner, *Langmuir* **2002**, *18*, 1518.
[28] *Diazald, MNNG, and Diazomethane Generators*, Aldrich Technical Information Bulletin Number AL-180, **1993**.

Meso/Macroporous Inorganic Oxide Monoliths from Polymer Foams**

By *Hideki Maekawa*, *Jordi Esquena*, *Samuel Bishop*, *Conxita Solans*, and *Bradley F. Chmelka**

A great deal of progress has recently been made in the development of synthesis and processing procedures for preparing ordered inorganic–organic composites or porous inorganic materials with uniform channel dimensions that can be adjusted over a wide range of length scales. Such materials are important for both fundamental study and their technological application in catalysis, micro- and opto-electronics, separations, etc. Ordered mesostructured inorganic solids have been prepared by using self-assembling surfactant agents, often low molecular weight or block copolymer amphiphiles to direct the structure of network-forming inorganic species.[1–6] Water-soluble inorganic species, for example, will preferentially associate with hydrophilic surfactant moieties through Coulombic or hydrogen-bonding interactions and be segregated and organized, according to the structure adopted by the self-as-

[*] Prof. B. F. Chmelka, Dr. H. Maekawa,[+] S. Bishop
Department of Chemical Engineering
University of California, Santa Barbara
CA 93106 (USA)
E-mail: bradc@engineering.ucsb.edu
Dr. J. Esquena, Dr. C. Solans
Institut d'Investigacions Químiques i Ambientals de Barcelona, CSIC
Jordi Girona, 18-26, E-08034 Barcelona (Spain)
[+] Present address: Department of Metallurgy, Graduate School of Engineering, Tohoku University, Sendai 980-8579, Japan.

[**] This work was supported by the US National Science Foundation through grant CTS-9871970 and a joint research project of the US–Spain Science and Technology Program 2000. Travel assistance was provided by the US NSF Division of International Programs through grant INT-9726744. We thank BASF for the donation of the F127 and P123 triblock copolymer species.

ADVANCED MATERIALS

sembling surfactant species. Characteristic ordering and dimensions of the inorganic material structure can be adjusted by modifying the composition and processing conditions used. In particular, by increasing the relative volume of the hydrophobic components, the characteristic size of the channel/cavity dimensions can be increased from less than 1 nm to tens of micrometers and larger. Examples of suitable structure-directing agents include molecular species used in zeolite synthesis,[7,8] low molecular weight and block copolymer surfactants,[9–15] emulsions,[16] and solid particles.[17–20]

By combining different structure-directing agents, co-assembled inorganic sol–gel precursors, and/or processing strategies, it has furthermore been possible to control the structures of composite and porous solids over a hierarchy of different independent length scales in the same material. Previously described methods to prepare materials with bimodal meso/macroporous structures have combined several of the above approaches. These have generally used self-assembling surfactant species in conjunction with larger scale agents, including solid particles,[21–24] fibrous bacteria,[25] a chitin-extracted natural polymer,[26] microemulsions,[27] or by macroscopic phase separations.[28–32] Challenges arise in the preparation of such bimodal meso/macroporous materials, such as avoiding a significant proportion of closed pores, controlling independently the sizes of the mesopores and the macropores, and managing the shrinkage of the whole structure while retaining the macroscopic shape.

Here, we describe the preparation of novel meso/macroporous inorganic oxide monoliths using a two-step procedure in which a molded polystyrene foam serves as a macroporous precursor scaffold for a mesostructure-forming sol–gel/amphiphilic block copolymer composite. Polystyrene foam monoliths are first formed by polymerization of styrene either in the continuous or the dispersed phase of highly concentrated water/oil emulsions. Afterwards, a self-assembling block-copolymer/sol–gel mixture is imbibed into the preformed macroporous foam. The macroporous structure depends on the morphology of the precursor foam, while mesostructural order is produced by self-assembly of the block copolymer surfactant and the inorganic species. Because the mesostructure-forming components are introduced after polymerization of a macrostructure-forming emulsion, the two meso/macro length scales can be adjusted independently. Consequently, the block copolymer and emulsion structure-directing agents do not interfere, with the result that processing conditions can be used that optimize separately the mesoscopic and macroscopic structures and bulk processability. Elimination of the organic agents by solvent extraction or calcination results in a dual meso/macroporous inorganic framework structure. This approach provides several advantages with respect to other methods described in the literature, including moldability of meso/macroporous inorganic oxide monoliths into different three-dimensional (3D) macroscopic bulk shapes, with independently adjustable bimodal pore size distributions.

Monolithic polystyrene foams were prepared by polymerizing styrene in highly concentrated water-in-oil (W/O) or oil-in-water (O/W) emulsions, as described in the literature.[33–39] The polystyrene foam monoliths prepared in the different emulsions have distinct macrostructures. As shown in Figure 1a, a representative polystyrene foam monolith obtained from a highly concentrated W/O emulsion, denoted as "W/O polystyrene", consisted of cellular macropores 0.5–3 μm in diameter, interconnected by windows approximately 0.1–1 μm diameter. The pore volume of the sample shown in Figure 1a was approximately 17 $cm^3 g^{-1}$, as measured by the amount of ethanol that was incorporated into the void spaces of the monolith at room temperature. In contrast, as shown in Figure 1c, a polystyrene foam monolith obtained from a highly concentrated O/W emulsion, denoted as "O/W polystyrene", consisted of small, densely packed polystyrene particles with an average diameter of 0.4 μm. The pore volume of this O/W-polystyrene foam was significantly smaller (~0.2 $cm^3 g^{-1}$) than the W/O-polystyrene sample. The morphologies and characteristic feature dimensions of the two polystyrene foam structures are similar to those reported in the literature for polymers prepared in W/O and O/W emulsions.[33,37–39]

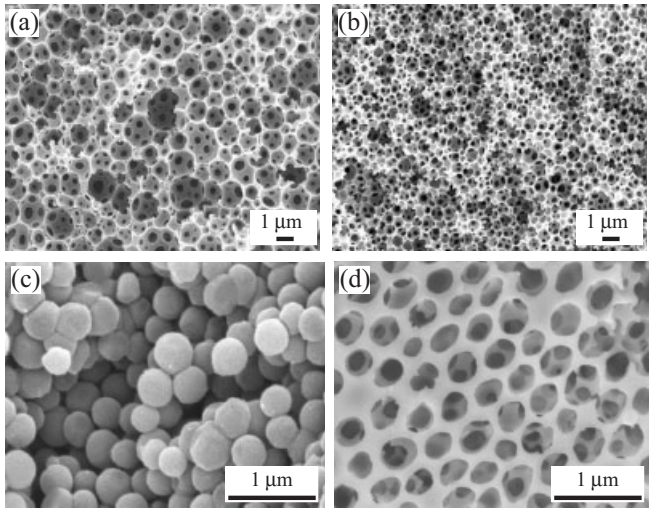

Fig. 1. SEM images of: a) a macroporous W/O-polystyrene foam monolith prepared from a highly concentrated water-in-oil emulsion containing 90 wt.-% persulfate solution, 2 wt.-% $C_{16}(EO)_6$, 4.8 wt.-% styrene, 1.2 wt.-% divinylbenzene, and 2 wt.-% tetradecane; b) calcined meso/macroporous silica prepared from the W/O-polystyrene monolith shown in (a) and a $EO_{20}PO_{70}EO_{20}$ (P123) triblock copolymer sol–gel solution consisting of 2 g TEOS, 0.7 g P123, 10 g ethanol, and 1.4 g H_2O (pH 0.7 (HCl)); c) a macroporous O/W-polystyrene foam monolith prepared from a highly concentrated oil-in-water emulsion (see Experimental); d) calcined meso/macroporous silica prepared from the O/W-polystyrene monolith shown in (c) and using the same sol–gel solution described in (b).

Mesostructural ordering, in combination with macroporosity, was introduced by using amphiphilic poly(ethylene oxide)-*b*-poly(propylene oxide)-*b*-poly(ethylene oxide) (PEO-PPO-PEO) triblock copolymers to direct the mesostructure of polymerizing metal oxide networks. This was achieved by imbibing the macroporous W/O- and O/W-polystyrene monoliths with ethanol sol–gel solutions containing soluble metal oxide precursors and PEO-PPO-PEO block copolymer surfactant species. Such sol–gel solutions were prepared in a simi-

lar way as described in the literature (see Experimental).[13,40] For the W/O-polystyrene foam, almost all of the free-pore volume of the polystyrene was filled with the block copolymer/sol–gel solution during the imbibition process, as revealed by the change in mass. For the O/W-polystyrene foams, however, removal of air was incomplete during imbibition of the sol–gel solution, indicating that some of the pores were inaccessible. After drying and aging the imbibed W/O-polystyrene foam, scanning electron microscopy (SEM) observations showed that its macropore surfaces were covered with silica/PEO-PPO-PEO films with thicknesses that depended on the concentration of the silica precursor. Finally, subsequent calcination to oxidize and remove the polystyrene and PEO-PPO-PEO triblock copolymer species yielded meso/macroporous silica.

Figures 1b,d show the respective SEM images of calcined meso/macroporous silica monoliths that were obtained from W/O-polystyrene (Fig. 1a) and O/W-polystyrene foams (Fig. 1c), respectively. The microscopic appearance of meso/macroporous silica obtained from W/O-polystyrene foam (Fig. 1b) is a replica of the W/O-polystyrene foam with shrinkage taken into account. The similarity of the polystyrene and subsequent silica macrostructures is due to the formation of PEO-PPO-PEO/silica films on the W/O-polystyrene macropore surfaces during the drying process, as the solvent (ethanol) evaporated. Removal of the organic polystyrene and block copolymer components by calcination results in a meso/macroporous silica framework that is a replica of the macroporous polystyrene foam structure. This is supported by nitrogen adsorption isotherm results, which yield (as determined from Barrett–Joyner–Halenda (BJH) pore size distribution analysis) a sharp peak at ~7 nm from the ordered mesopores, in addition to a broad peak in the range 150–500 nm and larger (not shown here).

On the other hand, meso/macroporous silica templated by the O/W-polystyrene foam, which consisted of aggregated particles approximately 400 nm in diameter (Fig. 1c), could not maintain the bulk shape of the precursor O/W-polystyrene monolith. This likely results from incomplete imbibition of the PEO-PPO-PEO/silica sol–gel solutions into the O/W-polystyrene foam, due to inaccessible macropores. However, as shown in Figure 1d, over localized regions the silica macroporous structure was the reverse of the O/W-polystyrene foam structures, similar to previous studies that used polystyrene particles as templates for forming macropores.[18–20] Large meso/macroporous silica or inorganic oxide monoliths with interconnected macropores are therefore preferably prepared using W/O-polystyrene foams as precursors.

Large and moldable meso/macroporous silica monoliths could be obtained by using W/O-polystyrene foams to control overall bulk shape and macropore structure. Examples of the bulk morphologies of the W/O-polystyrene foams and resultant meso/macroporous silicas are shown in Figure 2. Figures 2a,b show optical photographs of bulk-molded W/O-polystyrene monoliths with different shapes, while Figures 2c,d show the corresponding bulk meso/macroporous silica monoliths prepared from them. The centimeter scale bars indicate the sizes of the monoliths. During calcination to remove the organic components, densification of the silica networks also occurs, resulting in shrinkage of the monoliths compared to the dimensions of the original polystyrene foams. Such shrinkage appears to be uniform over microscopic and macroscopic length scales, resulting in approximately 25 % reduction in macropore and bulk monolith dimensions in the case of meso/macroporous silica. The bulk shapes of the calcined meso/macroporous silica monoliths otherwise appear to replicate the original W/O-polystyrene foams, as shown in Figure 2.

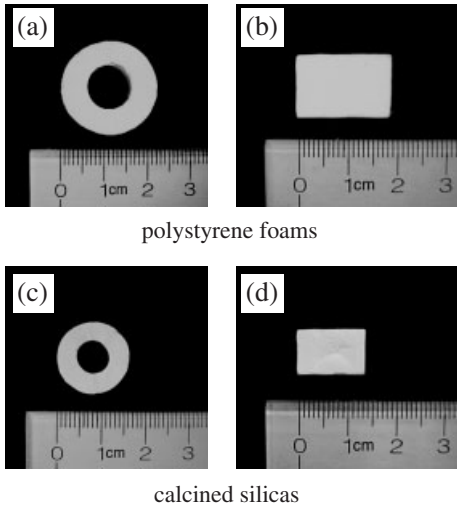

Fig. 2. Photographs of different bulk shapes of a,b) macroporous polystyrene imbibed with a block copolymer/silica sol–gel mixture and c,d) meso/macroporous silica. a) An annulus-shaped macroporous W/O-polystyrene monolith, prepared as described in Figure 1a; b) a rectangular macroporous W/O-polystyrene monolith prepared the same way as in (a); c,d) calcined meso/macroporous silica prepared by using the W/O-polystyrene monoliths shown in (a) and (b), respectively. The polystyrene foams and meso/macroporous silica were prepared as described in the Experimental section with the same solution formulations. The monoliths shown are approximately 1 cm thick in their dimensions normal to the page.

The shape of the macroporous polystyrene monoliths can be controlled and molded, according to the container used for the styrene-emulsion polymerization reaction. For instance, the ring-shaped monolith shown in Figure 2a was molded in the annular region between two concentric cylinders, while the rectangular monolith shown in Figure 2b adopted the shape of its rectangular container. Aside from shrinkage, these overall bulk shapes did not otherwise change during calcination. Thus, for both the W/O-polystyrene foams and subsequent meso/macroporous silica monoliths, substantial versatility exists with respect to the types of bulk shapes that can be formed. Moreover, the shapes of both the polystyrene and the silica monoliths can be modified by cutting with a sharp knife.

The macroscopic shrinkage and bulk densities of the meso/macroporous silica monoliths prepared from W/O-polystyrene foams are shown in Figure 3 as functions of silica weight percent in the precursor sol–gel solution. Densities as low as 0.05 g cm^{-3} could be obtained, which is comparable to typical

ADVANCED MATERIALS

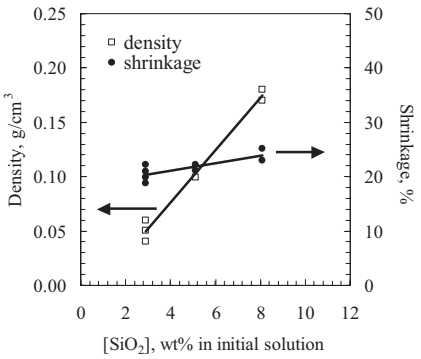

Fig. 3. Macroscopic shrinkage and bulk density of calcined meso/macroporous silica monoliths, plotted as functions of the SiO_2 concentration of the TEOS/water/ethanol/PEO-PPO-PEO triblock copolymer sol–gel solution imbibed into macroporous W/O-polystyrene foams, such as those shown in Figures 1a and 2a,b.

values, ~0.1 g cm^{-3}, for silica aerogels.[41] The extent of shrinkage is apparently independent of the relative SiO_2 concentration in the silica precursor solution, whereas the densities show a linear dependence that increases with SiO_2 weight percent. This suggests that the oxide framework increases in thickness for higher concentrations of silica in the precursor solution. Separate SEM images (not shown here) of meso/macroporous silicas support such an increase in wall thickness from approximately 50 to 200 nm and higher with increasing SiO_2 concentration. The polystyrene scaffold, highly crosslinked because it contains 20 wt.-% divinylbenzene, does not melt and supports the composite sample below its decomposition temperature in air (T_d ~ 300 °C). This apparently allows macroscopic shrinkage to occur uniformly, independent of the macropore wall thickness. This would otherwise be much more difficult to control for such thin silica framework structures.

The meso/macroporous silica monoliths prepared from the W/O-polystyrene foams and PEO-PPO-PEO triblock copolymer species (Figs. 1b and 2c,d) consisted of cellular macropores 0.3–2 μm in diameter, interconnected by windows approximately 0.2–0.5 μm in diameter with wall thicknesses of approximately 100 nm. The pore volumes were ~20 cm^3 g^{-1}, which is comparable to the pore volume of the precursor polymer foam (~17 cm^3 g^{-1}); the combination of additional mesoporosity and thinner silica walls apparently offset macroscopic shrinkage. The presence of ordered mesopores in the meso/macroporous silica monoliths is supported by the X-ray diffraction (XRD), N_2 sorption, and transmission electron microscopy (TEM) results shown in Figure 4. The XRD pattern in Figure 4a shows (100), (110), and (200) peaks associated with hexagonal arrays of cylindrical mesopores, with *d*-spacings of 6.8, 3.9, and 3.5 nm, respectively. The Brunauer–Emmett–Teller (BET) surface areas were between 250 and 750 m^2 g^{-1}. The higher surface areas correlate with higher TEOS concentrations and reduced macropore volumes, and are comparable to the surface areas observed for strictly mesoporous SBA-15 materials prepared using the same P123 PEO-PPO-PEO block copolymer species.[40] These surface

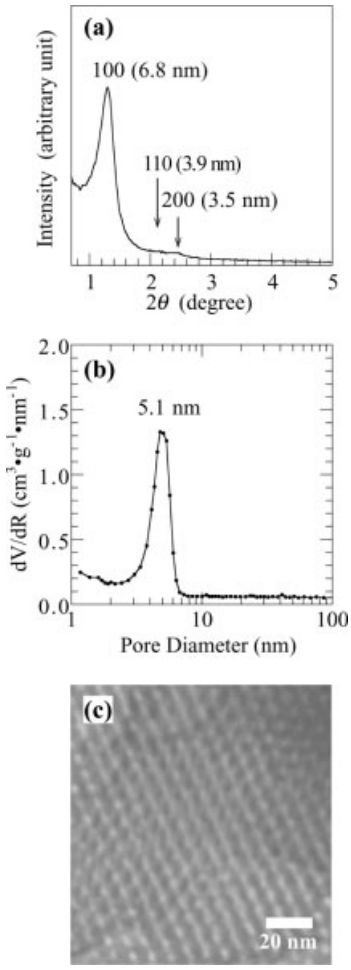

Fig. 4. a) Small-angle X-ray diffraction pattern, b) BJH pore size distribution curve obtained from the adsorption branch of N_2 adsorption isotherm measurements, and c) TEM image of the calcined meso/macroporous silica prepared from the W/O-polystyrene monolith. The imbibing sol–gel solution consisted of 2 g TEOS, 0.7 g P123, 20 g ethanol, and 1.6 g H_2O (pH 0.7 (HCl)).

areas are substantially higher than reported for strictly macroporous silica (< 50 m^2 g^{-1}).[18] The N_2 adsorption–desorption isotherm (not shown here) is Type IV, with a small hysteresis that indicates a minor deviation of the overall pore structure from a regular array of cylinders.[42] The pore diameter distribution curve shown in Figure 4b was obtained from the adsorption branch of the N_2 adsorption isotherm and calculated by the BJH method.[43] A sharply peaked distribution is observed at 5.1 ± 0.5 nm, reflecting a uniform mesopore size. In Figure 4c, the TEM image of the meso/macroporous silica monolith reveals hexagonal arrays of pores in the silica framework walls, with an estimated lattice spacing of 8 nm. This is in good agreement with the repeat distance ($a = d(100) \times 2/\sqrt{3}$ = 7.9 nm) determined from the *d*-spacing of the (100) XRD reflection. The mean pore wall thickness separating the ordered mesopores is estimated to be about 2.8 nm, which is comparable to that of hexagonal SBA-15 mesoporous silica prepared with P123 PEO-PPO-PEO triblock copolymer species.[14,40]

The methodology for preparing meso/macroporous inorganic oxide monoliths using polystyrene foams appears to be

extendable generally to metal oxide systems other than silica, including zirconia and titania. For example, Figures 5a,c and 5b,d respectively show the macropore structures and bulk shapes of a polystyrene foam scaffold and the resulting meso/macroporous zirconia monolith. Figures 5a,b respectively show SEM images of the macropores of a W/O-polystyrene foam monolith and resulting calcined meso/macroporous zirconia, prepared by an analogous procedure to that described for silica, but using $ZrCl_4$ as a precursor of zirconia. A 1.2 cm meso/macroporous zirconia half-disk with a thickness ≈ 1.5 mm (Fig. 5d) was obtained as a replica of the similarly shaped W/O-polystyrene foam (Fig. 5c). Comparing Figures 5c,d, the meso/macroporous zirconia monolith shrank by 40 %, approximately twice as much as the silica samples. This larger shrinkage may be due to different extents of framework densification or thinner macropore framework walls. As for the meso/macroporous silica, nearly uniform bulk shrinkage of meso/macroporous zirconia occurred, though with some heterogeneity appearing at the level of the macropores (Fig. 5b). Several cracks were observed in the meso/macroporous zirconia, though the monolith remained intact. The BET surface area of the meso/macroporous zirconia was measured to be 83 $m^2 g^{-1}$. The BJH pore size distribution curve, obtained from the adsorption branch of the N_2 sorption isotherm showed a sharp peak centered at 5 nm, with some evidence for small nanopores (< 2 nm).

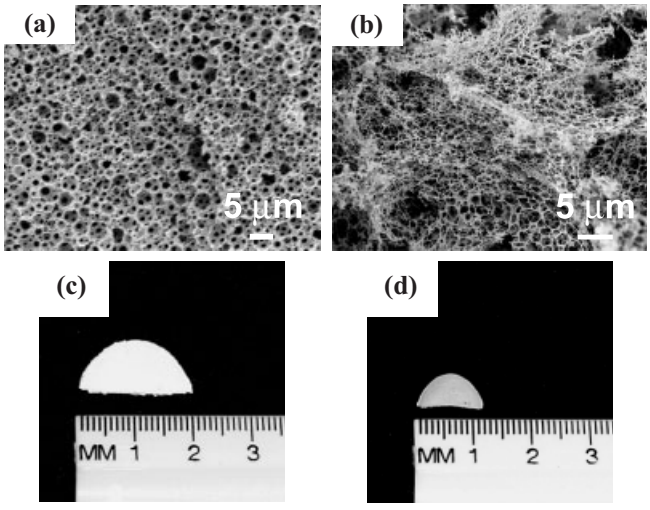

Fig. 5. a) SEM image of a W/O-polystyrene foam, prepared from a highly concentrated water-in-oil emulsion containing 90 wt.-% persulfate solution, 1.8 wt.-% $C_{16}(EO)_6$, 4.8 wt.-% styrene, 1.2 wt.-% divinylbenzene, 2 wt.-% tetradecane, and 0.2 wt.-% Synperonic L64. b) SEM image of calcined meso/macroporous zirconia prepared from the foam shown in (a). The zirconia solution consisted of 1.16 g $ZrCl_4$, 0.5 g P123, 7 g ethanol, and 0.2 g H_2O. c) Photograph of the W/O-polystyrene monolith. d) Photograph of the resulting calcined meso/macroporous zirconia monolith.

Monoliths of meso/macroporous titania up to 1.5 cm long were similarly prepared by using $Ti(OCH_2CH_3)_4$ as a precursor. Like the silica and zirconia analogs, the meso/macroporous titania monoliths shrank extensively (30 %) during calcination, independent of the concentration of the titania precursor species, similar to silica. The BET surface areas of meso/macroporous titania were 155–220 $m^2 g^{-1}$, with the BJH pore size distribution curves showing relatively broad peaks centered at 7 nm. This mesoscopic length scale is comparable to those obtained for pure mesoporous titania synthesized with $TiCl_4$ using the same PEO-PPO-PEO copolymers.[13] XRD results showed little long-range mesoscopic order for either the meso/macroporous titania or zirconia monoliths, which can likely be improved. The titania and zirconia frameworks remained amorphous following calcination at relatively low temperatures (350 °C and 400 °C, respectively). The results presented here suggest that the use of polymer foams as scaffolds for the preparation of monolithic mesoporous inorganic oxide materials is general. Such synthesis and processing strategies should enable the preparation of meso/macroporous inorganic solids with a wide variety of compositions, bimodal pore structures, dimensions, and bulk shapes.

In summary, the preparation and characterization of novel, moldable, low density meso/macroporous inorganic oxide monoliths have been described. Such materials were synthesized using macroporous polystyrene foams and PEO-PPO-PEO block copolymer species to direct the structures of network-forming metal oxide species. After calcination to remove the organic components, the resulting meso/macroporous silica, zirconia, and titania materials retained their macroscopic shapes and possessed independently adjustable meso- and macropore structures. For silica, the bimodal distributions of pore sizes were characterized to be uniform and highly ordered in the mesopore size regime 5–10 nm, with disordered 0.1–5 μm macropores. Such metal oxide monoliths with bimodal meso/macroporosities can be expected to combine reduced resistance to diffusion and high surface areas for adsorption and reaction, particularly for large molecular guest species. Combinations of pore sizes integrated into moldable monolithic materials have promise for yielding improved overall reaction, adsorption/separation, and/or structural properties.

Experimental

Materials: The surfactants hexaethyleneglycol *n*-hexadecyl ether, abbreviated as $C_{16}(OE)_6$ and octaethyleneglycol *n*-dodecyl ether, $C_{12}(OE)_8$, both 99+ %, were purchased from Nikko Chemicals Co. (Japan). The poly(ethylene oxide)-*block*-poly(propylene oxide)-*block*-poly(ethylene oxide) (PEO-PPO-PEO) triblock copolymer surfactants $(EO)_{20}(PO)_{70}(EO)_{20}$ (Pluronic P123) and $(EO)_{100}(PO)_{70}(EO)_{100}$ (Pluronic F127) were supplied by BASF (Mount Olive, NJ). $(EO)_{13}(PO)_{30}(EO)_{13}$ (Synperonic L64) was purchased from ICI (Kortenberg, Belgium). $C_{18}(EO)_{100}$ (Brij 700) was supplied by Sigma-Aldrich Chemie (Steinheim, Germany). All surfactants were used as received. Monomers, initiators, electrolytes, and tetradecane were purchased either from Aldrich (Milwaukee, Wisconsin) or from Merck (Mollet, Barcelona, Spain). Styrene and divinylbenzene were purified by distillation under vacuum or by passing through neutral chromatographic aluminum oxide to eliminate the inhibitor 4-*tert*-butylpyrocatechol. Potassium persulfate (99 %), initiator, potassium nitrate (99+ %), used to stabilize the emulsions, and tetradecane (99+ %), used to control the emulsion phase-inversion temperatures of the emulsions, were used as received. The oil-soluble initiator 2,2-azobisisobutyronitrile (AIBN), used to polymerize O/W emulsions, was purified by recrystallization in methanol. Deionized water was used in all of the experiments. Inorganic oxide precursors tetraethylorthosilicate (TEOS, 98+ %), tetraethylorthotitanate (TEOT, ≈ 95 %), and zirconi-

ADVANCED MATERIALS

um(IV) chloride (99.9+ %) were purchased from Aldrich. Concentrated aqueous hydrochloric acid, 37 %, was purchased from EM Science (Gibbstown, NJ) and absolute ethanol from either Merck or Gold Shield Chemical (Hayward, California).

Preparation of Macroporous Polystyrene Monoliths: For the highly concentrated W/O emulsions, the 90 wt.-% dispersed aqueous phase contained the radical initiator $K_2S_2O_8$ with the mass ratio $H_2O/K_2S_2O_8$ = 900:1. In typical preparations, 2 wt.-% surfactant was used, with surfactant mass ratios $C_{16}(OE)_6$/$C_{12}(OE)_8$ ranging from 7:3 to 10:0. Divinylbenzene (DVB) was added to the styrene in the mass ratio styrene/DVB = 4:1 to promote crosslinking and thus greater mechanical strength of the resultant polystyrene foam [38]. Between 5 and 6 wt.-% monomer was used, with tetradecane respectively present between 3 and 2 wt.-%. The total oil (monomer plus tetradecane) was kept constant at 8 wt.-%. Synperonic L64 was added at 0.2 wt.-% to enhance the stability of the emulsions. Highly concentrated emulsions were formed by rapidly increasing the temperature from 0 to 60 °C, while keeping the samples under agitation [38,44,45]. Samples were then placed in molds and maintained at 60 °C for 48 h, during which time polymerization of the styrene occurred. The wet polystyrene monoliths were removed from their molds by carefully breaking the glass containers, after which they were washed twice with water and twice with ethanol, both at 60 °C, to remove tetradecane and the surfactant species.

For the highly concentrated O/W emulsions, the composition in a typical preparation was: water 18 wt.-%, $C_{18}(OE)_{100}$ 0.9 wt.-%, Synperonic L64 0.1 wt.-%, KNO_3 2 wt.-%, styrene 78 wt.-%, and AIBN 1 wt.-%. The O/W emulsions were prepared at constant temperature by the multiple-emulsion method [39,46]. The samples were kept under moderate stirring at room temperature; a sharp increase in sample viscosity indicated the formation of a concentrated emulsion. The samples were placed in molds to polymerize the styrene and treated as described for the W/O foams above.

Preparation of Meso/Macroporous Inorganic Oxide Monoliths: Bimodal meso/macrostructured inorganic oxide monoliths were prepared by imbibing macroporous polystyrene foams with an acidic sol–gel solution containing amphiphilic PEO-PPO-PEO surfactant species as structure-directing agents. Conditions for preparing the block copolymer-organized oxide mesostructures were similar to those previously described in the literature [13,40]. For meso/macroporous silica, a typical composition of the inorganic precursor solutions was as follows: 0.3–1.0 g P123 or F127, 1.86 or 11.5 g TEOS, 1.4 g H_2O, and 4–16 g ethanol. The pH of the solution was adjusted to be between pH 0.7 and pH 1.5 by the addition of HCl. For meso/macroporous titania, the precursor solutions were prepared by dissolving 1.15 g of P123, 1.94 mL of TEOT, 1.35 mL HCl, and 2–10 g of ethanol. For meso/macroporous zirconia, the precursor solutions contained 0.5 g of P123, 7 g of ethanol, 1.16 g $ZrCl_4$, and 0.2–1.0 g of water. The solutions were imbibed into the macroporous polystyrene foam monoliths by using large syringes and removing the air from the monoliths under modest vacuum. The imbibed foams were aged for 24–72 h, at room temperature, during which time polymerization of the inorganic oxide species occurred. The resulting silica composite was dried for 24 h at 25 °C and then calcined at 500 °C in air for 6 h to yield mesoscopically ordered meso/macroporous silica. The titania composite was dried for 48 h, heated and held at 60 °C for 24 h, and then calcined in air at 350 °C for 24 h to yield meso/macroporous titania. The zirconia composite was dried for 24 h and calcined at 400 °C for 24 h to yield meso/macroporous zirconia. The polystyrene and triblock copolymer surfactants were eliminated during calcination to yield inorganic oxide monoliths with dual meso/macroporous structures, whose length scales were separately established by the hydrophobic block copolymer and polystyrene foam structures, respectively.

Characterization: SEM images were obtained by using a JEOL 6300 microscope. Samples were coated with a gold layer approximately 25 nm thick by sputtering. TEM images were acquired on a JEOL 2000 electron microscope operating at 200 keV. Powder XRD patterns were acquired on a Scintag PADX diffractometer using Cu Kα radiation. After the samples were vacuum-dried at 473 K overnight, nitrogen adsorption/desorption isotherms were measured at 77 K using a Micromeritics ASAP 2000 system. Specific surface areas were measured using the BET method, and pore size distributions were obtained from the analysis of the adsorption branch of the isotherm using the BJH model.

Received: July 29, 2002
Final version: December 16, 2002

[1] A. Sayari, P. Liu, *Microporous Mater.* **1997**, *12*, 149.
[2] D. Zhao, P. Yang, Q. Huo, B. F. Chmelka, G. D. Stucky, *Current Opin. Solid State Mater. Sci.* **1998**, *3*, 111.
[3] I. Soten, G. A. Ozin, *Current Opin. Colloid Interface Sci.* **1999**, *4*, 325.
[4] P. Yang, D. Zhao, D. I. Margolese, B. F. Chmelka, G. D. Stucky, *Chem. Mater.* **1999**, *11*, 2813.
[5] U. Ciesla, F. Schüth, *Microporous Mesoporous Mater.* **1999**, *27*, 131.
[6] T. J. Barton, L. M. Bull, W. G. Klemperer, D. A. Loy, B. McEnaney, M. Misono, P. A. Monson, G. Pez, G. W. Scherer, J. C. Vartuli, O. M. Yaghi, *Chem. Mater.* **1999**, *11*, 2633.
[7] S. I. Zones, Y. Nakagawa, G. S. Lee, C. Y. Chen, L. T. Yuen, *Microporous Mesoporous Mater.* **1998**, *21*, 199.
[8] A. K. Cheetham, G. Ferey, T. Loiseau, *Angew. Chem. Int. Ed.* **1999**, *38*, 3269.
[9] C. T. Kresge, M. E. Leonowicz, W. J. Roth, J. C. Vartuli, J. S. Beck, *Nature* **1992**, *359*, 710.
[10] S. A. Bagshaw, E. Prouzet, T. J. Pinnavaia, *Science* **1995**, *269*, 1242.
[11] C. G. Göltner, M. Antonietti, *Adv. Mater.* **1997**, *9*, 431.
[12] D. Zhao, J. L. Feng, Q. S. Huo, N. Melosh, G. H. Fredrickson, B. F. Chmelka, G. D. Stucky, *Science* **1998**, *279*, 548.
[13] P. Yang, D. Zhao, D. I. Margolese, B. F. Chmelka, G. D. Stucky, *Nature* **1998**, *396*, 152.
[14] N. A. Melosh, P. Lipic, F. S. Bates, F. Wudl, G. D. Stucky, G. H. Fredrickson, B. F. Chmelka, *Macromolecules* **1999**, *32*, 4332.
[15] P. F. W. Simon, R. Ulrich, H. W. Spiess, U. Wiesner, *Chem. Mater.* **2001**, *13*, 3464.
[16] A. Imhof, D. J. Pine, *Nature* **1997**, *389*, 948.
[17] J. E. G. J. Wijnhoven, W. L. Vos, *Science* **1998**, *281*, 802.
[18] B. T. Holland, C. F. Blanford, A. Stein, *Science* **1998**, *281*, 538.
[19] G. Subramanian, V. N. Manoharan, J. D. Thorne, D. J. Pine, *Adv. Mater.* **1999**, *11*, 1261.
[20] P. Jiang, G. N. Ostojic, R. Narat, D. M. Mittleman, V. L. Colvin, *Adv. Mater.* **2001**, *13*, 389.
[21] M. Antonietti, B. Berton, C. Göltner, H. P. Hentze, *Adv. Mater.* **1998**, *10*, 154.
[22] P. Yang, T. Deng, D. Zhao, P. Feng, D. Pine, B. F. Chmelka, G. M. Whitesides, G. D. Stucky, *Science* **1998**, *282*, 2244.
[23] B. T. Holland, L. Abrams, A. Stein, *J. Am. Chem. Soc.* **1999**, *121*, 4308.
[24] C. J. H. Jacobsen, C. Madsen, J. Houzvicka, I. Schmidt, A. Carlsson, *J. Am. Chem. Soc.* **2000**, *122*, 7116.
[25] S. A. Davis, S. L. Burkett, N. H. Mendelson, S. Mann, *Nature* **1997**, *385*, 420.
[26] V. Pedroni, P. C. Schulz, M. E. Gschaider de Ferreira, M. A. Morini, *Colloid Polym. Sci.* **2000**, *278*, 964.
[27] P. Schmidt-Winkel, W. W. Lukens, P. Yang, D. I. Margolese, J. S. Lettow, J. Y. Ying, G. D. Stucky, *Chem. Mater.* **2000**, *12*, 686.
[28] P. Schmidt-Winkel, P. Yang, D. I. Margolese, B. F. Chmelka, G .D. Stucky, *Adv. Mater.* **1999**, *11*, 303.
[29] S. Schacht, Q. Huo, I. G. Voigt-Martin, G. D. Stucky, F. Schüth, *Science* **1996**, *273*, 768.
[30] N. Ishizuka, H. Minakuchi, K. Nakanishi, N. Soga, N. Tanaka, *J. Chromatogr. A* **1998**, *797*, 133.
[31] D. Zhao, P. Yang, B. F. Chmelka, G. D. Stucky, *Chem. Mater.* **1999**, *11*, 1174.
[32] R. Takahashi, S. Sato, T. Sodesawa, K. Suzuki, M. Tafu, K. Nakanishi, N. Soga, *J. Am. Ceram. Soc.* **2001**, *84*, 1968.
[33] D. Barby, Z. Haq (Unilever), *European Patent 0060 138*, **1982**.
[34] J. M. Williams, *Langmuir* **1988**, *4*, 44.
[35] J. M. Williams, A. J. Gray, M. H. Wilkerson, *Langmuir* **1990**, *6*, 437.
[36] E. Ruckenstein, J. S. Park, *Polymer* **1992**, *33*, 405.
[37] E. Ruckenstein, *Adv. Polym. Sci.* **1997**, *127*, 1.
[38] J. Esquena, G. S. R. R. Sankar, C. Solans, *Langmuir* **2003**, *19*, in press.
[39] J. Esquena, C. Solans, *Jorn. Com. Esp. Deterg.* **2001**, *31*, 203.
[40] D. Zhao, Q. S. Huo, J. L. Feng, B. F. Chmelka, G. D. Stucky, *J. Am. Chem. Soc.* **1998**, *120*, 6024.
[41] N. Hüsing, U. Schubert, *Angew. Chem. Int. Ed.* **1998**, *37*, 23.
[42] P. J. Branton, P. G. Hall, K. S. W. Sing, H. Reichert, F. Schüth, K. K. Unger, *J. Chem. Soc. Faraday Trans.* **1994**, *90*, 2965.
[43] E. P. Barrett, L. G. Joyner, P. P. Halenda, *J. Am. Chem. Soc.* **1951**, *73*, 373.
[44] R. Pons, I. Carrera, P. Erra, H. Kunieda, C. Solans, *Colloids Surf., A* **1994**, *91*, 259.
[45] H. Kunieda, Y. Fukui, H. Uchiyama, C. Solans, *Langmuir* **1996**, *12*, 2136.
[46] C. Solans, R. Pons, H. Kunieda, in *Modern Aspects of Emulsion Science* (Ed: B. P. Binks), Royal Society of Chemistry, Cambridge **1998**, p. 367.

